Supporting Information

Syntheses of Ferrocene-Functionalized Indium-based Metal-Organic Frameworks for Third Order Nonlinear Optical Application

Rong Zhang[a,b], Bing Wang[a,b], Fei Wang[b*], Shumei Chen[a*] and Jian Zhang[b]

[a] College of Chemistry, Fuzhou University, Fuzhou, Fujian 350108, P. R. China. E-mail: csm@fzu.edu.cn.

[b] State Key Laboratory of Structural Chemistry, Fujian Institute of Research on the Structure of Matter, the Chinese Academy of Sciences, Fuzhou, Fujian 350002, P. R. China. E-mail: wangfei04@fjirsm.ac.cn.

Contents

Photocurrent measurement

We prepared the working electrode by solution coating method as follows: the newly prepared sample (5 mg) and Nafion (10 μL) dissolved in 0.5 mL ethanol with ultrasound and 40 μL solution was uniformly dropped on clean FTO conductive glass (1.0 × 4.0 cm^2, 10 $\Omega \cdot cm^{-2}$). The photocurrent experiment was carried out on the CHI760E electrochemical workstation of the three electrode system, in which Pt sheet was the counter electrode and Ag/AgCl electrode was the reference electrode. The experiment was carried out in 0.2 M Na_2SO_4 electrolyte at room temperature, and a 300 W high-pressure xenon lamp (full band) was used as a visible light source.

Cyclic voltammetric measurement

We prepared the working electrode by solution coating method as follows: the newly prepared sample (5 mg) and Nafion (10 μL) dissolved in 0.5 ml ethanol with ultrasound and 40 μL solution was uniformly dropped on clean FTO conductive glass (1.0 × 4.0 cm^2, 10 $\Omega \cdot cm^{-2}$). The photocurrent experiment was carried out on the CHI760E electrochemical workstation of the three electrode system, in which Pt sheet was the counter electrode and Ag/AgCl electrode was the reference electrode. The experiment was carried out in 0.2 M Na_2SO_4 electrolyte at room temperature, and CV cycles were measured at scan rate of 50 $mV \cdot s^{-1}$.

Single crystal synthesis and characterization of compounds

Single crystal structure determination

Table S1. Crystal data and structure refinement for compounds **1** to **7**.

Compounds	**1**	**2**	**3**	**4**
Formula	$C_{86}H_{74}Fe_3In_2O_{21}P_2$	$C_{48}H_{46}Fe_2InO_{13}P$	$C_{24}FeInN_2O_9H_{19}$	$C_{29}H_{26}ClFeInN_3O_6S$
Weight	1902.58	1088.34	650.08	750.71
Crystal system	monoclinic	monoclinic	orthorhombic	monoclinic
Space group	*C*2/*c*	$P2_1/c$	*Pnna*	*P*2/*c*
a/Å	16.14000(10)	10.17060(10)	9.5846(15)	12.5179(3)
b/Å	15.74500(10)	20.3048(2)	10.3814(18)	13.4210(5)
c/Å	29.8741(2)	21.23650(10)	24.795(2)	17.7970(7)
α/°	90	90	90	90

β/°	101.4600(10)	91.3550(10)	90	95.078(3)
γ/°	90	90	90	90
Volume/Å^3	7440.38(9)	4384.37(6)	2467.2(6)	2978.21(18)
Z	4	4	4	4
ρ_{calc}g/cm^3	1.698	1.649	1.75	1.674
GOOF	1.056	1.034	1.091	1.085
Final R indexes [I>=2σ (I)]	R_1 = 0.0314, wR_2 = 0.0846	R_1 = 0.0445, wR_2 = 0.1065	R_1 = 0.0916, wR_2 = 0.1718	R_1 = 0.0696, wR_2 = 0.2119
Final R indexes [all data]	R_1 = 0.0333, wR_2 = 0.0857	R_1 = 0.0509, wR_2 = 0.1097	R_1 = 0.1273, wR_2 = 0.1877	R_1 = 0.0803, wR_2 = 0.2253
CCDC No.	2204902	2204903	2204897	2204900

Compounds	**5**	**6**	**7**
Formula	$C_{37}H_{28}ClFeInO_6P$	$C_{36}H_{32}Cl_2FeInO_6P$	$C_{15}H_{13}FeInN_2O_5$
Weight	805.68	833.15	471.94
Crystal system	triclinic	monoclinic	orthorhombic
Space group	*P*-1	$P2_1/c$	*Pbca*
a/Å	10.1386(3)	10.27250(10)	18.1609(7)
b/Å	12.2014(4)	28.3286(4)	9.7351(5)
c/Å	13.8268(3)	11.8384(2)	22.3468(10)
α/°	79.370(2)	90	90
β/°	87.630(2)	101.0380(10)	90
γ/°	84.833(2)	90	90
Volume/Å^3	1673.73(8)	3381.31(8)	3950.9(3)
Z	2	4	8
ρ_{calc}g/cm^3	1.599	1.637	1.587
GOOF	1.022	1.049	1.107
Final R indexes [I>=2σ (I)]	R_1 = 0.0868, wR_2 = 0.2099	R_1 = 0.0356, wR_2 = 0.0951	R_1 = 0.0752, wR_2 = 0.1712
Final R indexes [all data]	R_1 = 0.1506, wR_2 = 0.2302	R_1 = 0.0447, wR_2 = 0.1000	R_1 = 0.1058, wR_2 = 0.1923
CCDC No.	2204899	2204898	2204901

Table S2. Selected bond lengths (Å) and angles (°) for **1**.

In1-O11	2.251(2)	O2ii-In1-O4	150.39(7)
In1-O8^{i}	2.242(2)	O2ii-In1-O10	126.82(8)
In1-O2^{ii}	2.273(2)	O3-In1-O11	97.46(9)
In1-O3	2.154(2)	O3-In1-O8^{i}	90.59(8)
In1-O9	2.189(2)	O3-In1-O2ii	139.56(8)
In1-O1^{ii}	2.295(2)	O3-In1-O9	136.50(8)
In1-O4	2.572(2)	O3-In1-O1^{ii}	82.41(8)
In1-O10	2.404(3)	O3-In1-O4	54.69(8)
O11-In1-O2^{ii}	83.83(8)	O3-In1-O10	83.84(8)
O11-In1-O1^{ii}	83.30(9)	O9-In1-O11	106.72(9)
O11-In1-O4	123.83(8)	O9-In1-O8^{i}	75.63(7)
O11-In1-O10	55.70(9)	O9-In1-O2^{ii}	79.71(8)
O8i-In1-O11	164.26(9)	O9-In1-O1^{ii}	135.08(8)
O8i-In1-O2^{ii}	81.29(7)	O9-In1-O4	81.84(7)
O8i-In1-O1^{ii}	84.40(8)	O9-In1-O10	80.93(8)
O8i-In1-O4	71.79(7)	O1ii-In1-O4	129.28(7)
O8i-In1-O10	139.12(8)	O1ii-In1-O10	134.31(8)
O2ii-In1-O1^{ii}	57.48(7)	O10-In1-O4	72.10(8)

Symmetry codes: (i) -x+1, y, -z+1/2; (ii) -x+3/2, y-1/2, -z+1/2.

Table S3. Selected bond lengths (Å) and angles (°) for **2**.

In1-O6^{i}	2.244(2)	O4-In1-O3	57.33(8)
In1-O4	2.260(2)	O7^{i}-In1-O4	77.86(8)
In1-O7^{i}	2.248(2)	O7^{i}-In1-O5^{ii}	131.43(8)
In1-O5^{ii}	2.275(2)	O7^{i}-In1-O8^{ii}	84.98(9)
In1-O8^{ii}	2.272(2)	O7^{i}-In1-O3	122.30(8)
In1-O2	2.141(2)	O5^{ii}-In1-O3	84.17(8)
In1-O3	2.313(2)	O8^{ii}-In1-O5^{ii}	57.59(9)
O6^{i}-In1-O4	90.21(8)	O8^{ii}-In1-O3	141.40(9)
O6^{i}-In1-O7^{i}	58.71(9)	O2-In1-O6^{i}	167.75(10)
O6^{i}-In1-O5^{ii}	87.87(8)	O2-In1-O4	87.14(9)
O6i-In1-O8^{ii}	88.15(8)	O2-In1-O7^{i}	132.00(10)
O6^{i}-In1-O3	85.13(8)	O2-In1-O5^{ii}	86.78(9)
O4-In1-O5^{ii}	141.46(9)	O2-In1-O8^{ii}	98.23(9)
O4-In1-O8^{ii}	160.80(9)	O2-In1-O3	83.38(9)

Symmetry codes: (i) x, -y+1/2, z+1/2; (ii) x+1, y, z.

Table S4. Selected bond lengths (Å) and angles (°) for **3**.

In1-O3	2.201(6)	O4^{iii}-In1-O1^{i}	74.9(2)
In1-O3^{i}	2.201(6)	O4^{iii}-In1-O1	125.7(3)
In1-O4^{ii}	2.236(6)	O4^{ii}-In1-O1^{i}	125.7(3)
In1-O4^{iii}	2.236(6)	O4^{ii}-In1-O1	74.9(2)
In1-O2	2.170(7)	O2^{i}-In1-O3	150.6(3)
In1-O2^{i}	2.170(7)	O2^{i}-In1-O3^{i}	91.7(3)
In1-O1^{i}	2.582(10)	O2-In1-O3	91.7(3)
In1-O1	2.582(10)	O2-In1-O3^{i}	150.6(3)
O3-In1-O3^{i}	97.9(3)	O2^{i}-In1-O4^{iii}	128.2(3)
O3^{i}-In1-O4^{iii}	74.0(2)	O2-In1-O4^{ii}	128.2(3)
O3-In1-O4^{iii}	81.2(2)	O2-In1-O4^{iii}	80.2(3)
O3^{i}-In1-O4^{ii}	81.2(2)	O2^{i}-In1-O4^{ii}	80.2(3)
O3-In1-O4^{ii}	74.0(2)	O2-In1-O2^{i}	93.3(4)
O3-In1-O1^{i}	156.0(2)	O2^{i}-In1-O1^{i}	53.4(3)
O3^{i}-In1-O1^{i}	74.6(2)	O2-In1-O1	53.4(3)
O3-In1-O1	74.6(2)	O2-In1-O1^{i}	85.4(3)
O3^{i}-In1-O1	156.0(2)	O2^{i}-In1-O1	85.4(3)
O4^{ii}-In1-O4^{iii}	141.8(3)	O1^{i}-In1-O1	120.9(3)

Symmetry codes: (i) -x+1/2, -y+1, z; (ii) -x+1, -y+1, -z+1; (iii) x-1/2, y, -z+1.

Table S5. Selected bond lengths (Å) and angles (°) for **4**.

In1-Cl1	2.3940(18)	O3-In1-Cl1	98.19(13)
In1-O2	2.346(5)	O3-In1-O2	79.66(17)
In1-O4^{i}	2.206(5)	O3-In1-O5^{ii}	133.17(18)
In1-O3	2.216(4)	O3-In1-O6^{ii}	78.38(18)
In1-O5^{ii}	2.287(5)	O5^{ii}-In1-Cl1	100.89(13)
In1-O1	2.208(5)	O5^{ii}-In1-O2	141.73(17)
In1-O6^{ii}	2.292(5)	O5^{ii}-In1-O6^{ii}	57.42(17)
O2-In1-Cl1	90.74(13)	O1-In1-Cl1	98.04(14)
O4^{i}-In1-Cl1	173.08(12)	O1-In1-O2	57.79(16)
O4^{i}-In1-O2	84.94(18)	O1-In1-O3	134.37(18)
O4^{i}-In1-O3	75.74(17)	O1-In1-O5^{ii}	84.36(17)
O4^{i}-In1-O5^{ii}	85.81(17)	O1-In1-O6^{ii}	141.13(18)
O4^{i}-In1-O1	84.24(17)	O6^{ii}-In1-Cl1	96.11(14)
O4^{i}-In1-O6^{ii}	86.01(18)	O6^{ii}-In1-O2	157.71(17)

Symmetry codes: (i) -x, -y+1, -z+1; (ii) x, -y+1, z-1/2.

Table S6. Selected bond lengths (Å) and angles (°) for **5**.

In01-Cl03	2.4725(17)	O007-In01-Cl03	99.44(14)
In01-O005^{i}	2.236(4)	O007-In01-O005^{i}	85.76(17)
In01-O006^{ii}	2.233(5)	O007-In01-O006^{ii}	85.78(16)
In01-O007	2.195(4)	O007-In01-O008^{ii}	142.46(18)
In01-O008^{ii}	2.321(4)	O007-In01-O009	134.06(18)

In01-O009	2.219(5)	O007-In01-O001	57.26(17)
In01-O001	2.320(5)	O008^{ii}-In01-Cl03	90.67(14)
O005^{i}-In01-Cl03	174.79(11)	O009-In01-Cl03	101.57(13)
O005^{i}-In01-O008^{ii}	85.03(17)	O009-In01-O005^{i}	74.66(17)
O005^{i}-In01-O001	93.50(17)	O009-In01-O006^{ii}	131.02(16)
O006^{ii}-In01-Cl03	96.64(13)	O009-In01-O008^{ii}	77.53(18)
O006^{ii}-In01-O005i	83.49(17)	O009-In01-O001	82.51(17)
O006^{ii}-In01-O008ii	57.04(17)	O001-In01-Cl03	89.51(14)
O006^{ii}-In01-O001	143.04(16)	O001-In01-O008^{ii}	159.66(18)

Symmetry codes: (i) -x+2, -y, -z+2; (ii) x+1, y, z.

Table S7. Selected bond lengths (Å) and angles (°) for **6**.

In1-Cl2	2.4868(8)	O5-In1-O2^{i}	163.77(9)
In1-Cl1	2.4774(9)	O5-In1-O4	84.30(10)
In1-O006	2.343(3)	O3^{i}-In1-Cl2	90.78(7)
In1-O5	2.244(2)	O3^{i}-In1-Cl1	89.55(7)
In1-O3^{i}	2.252(2)	O3^{i}-In1-O006	82.25(9)
In1-O2^{i}	2.327(3)	O3^{i}-In1-O2^{i}	56.94(9)
In1-O4	2.268(3)	O3^{i}-In1-O4	136.70(10)
Cl1-In1-Cl2	179.16(3)	O2^{i}-In1-Cl2	88.73(7)
O006-In1-Cl2	91.64(6)	O2^{i}-In1-Cl1	90.81(7)
O006-In1-Cl1	89.17(7)	O2^{i}-In1-O006	139.19(8)
O5-In1-Cl2	87.98(7)	O4-In1-Cl2	91.74(7)
O5-In1-Cl1	92.27(7)	O4-In1-Cl1	87.49(7)
O5-In1-O006	56.83(8)	O4-In1-O006	140.82(10)
O5-In1-O3^{i}	138.99(9)	O4-In1-O2^{i}	79.92(10)

Symmetry codes: (i) x+1, y, z.

Table S8. Hydrogen bond parameters for **6**.

D-H-A	d(D-H)/Å	d(H-A)/Å	d(D-A)/Å	D-H-A/°
O4-H4B-O006^{i}	0.87	2.02	2.773(4)	144.5
O1-H1A-O3^{ii}	0.87	2.11	2.964(4)	168.4

Symmetry codes: (i) x, 1/2-y, -1/2+z; (ii) 1-x, 1-y, 2-z.

Table S9. Selected bond lengths (Å) and angles (°) for **7**.

In1-O1	2.224(6)	O3^{i}-In1-O5^{i}	56.0(2)
In1-O2	2.292(6)	O3^{i}-In1-C1^{i}	28.2(3)
In1-O3^{i}	2.303(6)	O4-In1-C1^{i}	163.0(3)
In1-O4	2.366(6)	O5^{i}-In1-O4	169.1(2)
In1-O5^{i}	2.344(7)	O5^{i}-In1-C1^{i}	27.8(3)
In1-N1	2.190(7)	N1-In1-O1	91.0(3)

In1-N2^{ii}	2.197(6)	N1-In1-O2	140.8(2)
In1-C1^{i}	2.691(9)	N1-In1-O3^{i}	140.5(2)
O1-In1-O2	87.0(3)	N1-In1-O4	84.6(2)
O1-In1-O3^{i}	88.8(3)	N1-In1-O5^{i}	84.6(2)
O1-In1-O4	90.2(3)	N1-In1-N2^{ii}	93.4(3)
O1-In1-O5^{i}	89.1(3)	N1-In1-C1i	112.4(3)
O1-In1-C1^{i}	88.1(3)	N2^{ii}-In1-O1	174.8(3)
O2-In1-O3^{i}	78.6(2)	N2^{ii}-In1-O2	87.8(3)
O2-In1-O4	56.3(2)	N2^{ii}-In1-O3^{i}	89.6(2)
O2-In1-O5^{i}	134.5(2)	N2^{ii}-In1-O4	87.4(2)
O2-In1-C1^{i}	106.7(3)	N2^{ii}-In1-O5^{i}	94.2(3)
O3^{i}-In1-O4	134.9(2)	N2^{ii}-In1-C1^{i}	92.8(3)

Symmetry codes: (i) -x+1, -y+1, -z+1; (ii) -x+1/2, y-1/2.

Infrared spectrum analysis

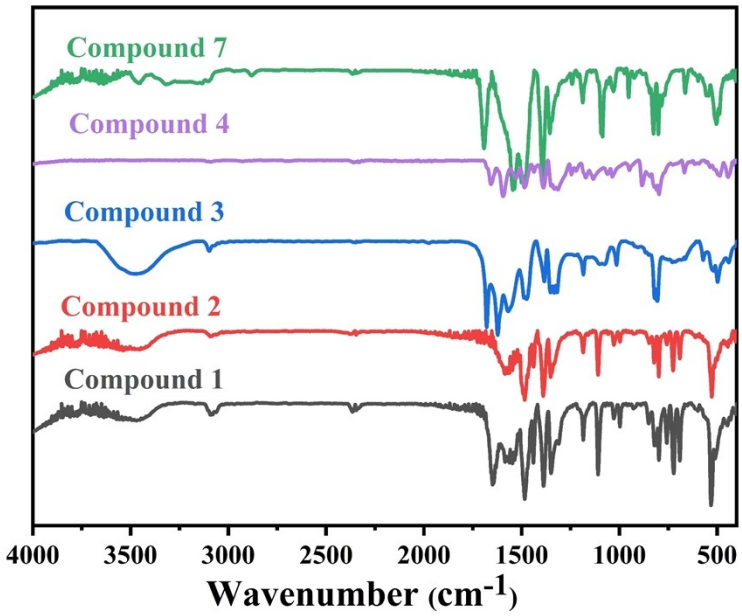

Figure S1. Infrared (IR) spectroscopy of **1** to **4** and **7**.

^{1}H NMR spectra

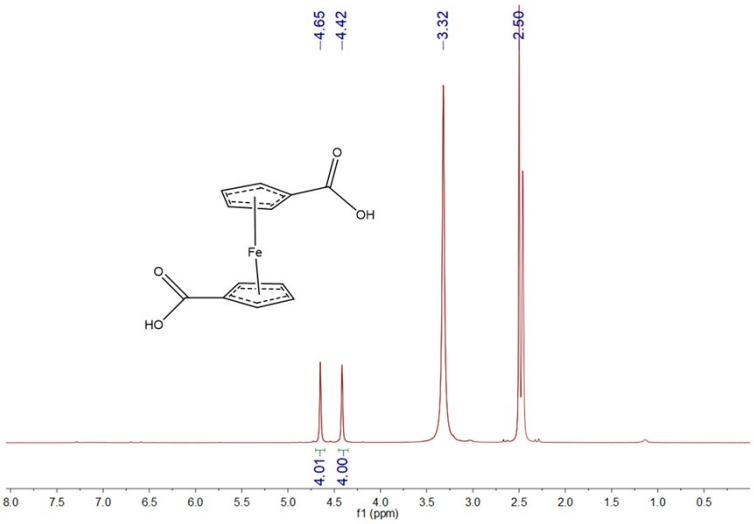

Figure S2. ^{1}H NMR spectra of the H_2FcDCA: ^{1}H NMR (400 MHz, DMSO-d_6) δ 4.65 (s, 4H), 4.42 (s, 4H).

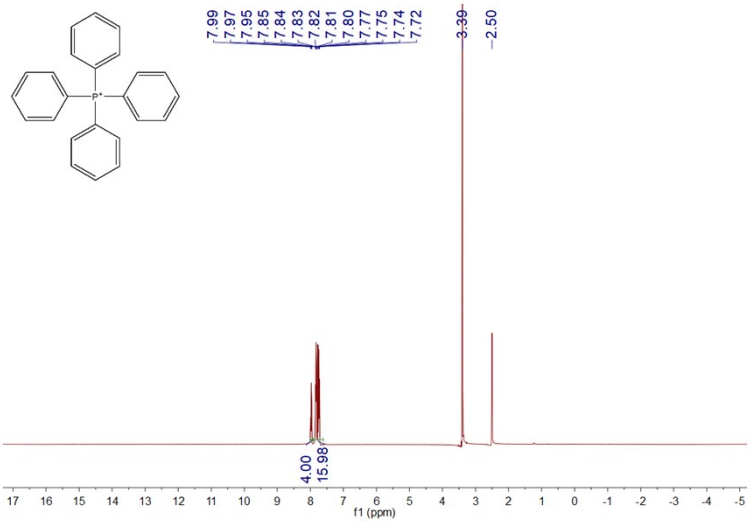

Figure S3. ^{1}H NMR spectra of the TPP^+: ^{1}H NMR (400 MHz,) δ 7.97 (t, J = 7.5 Hz, 4H), 7.85 – 7.72 (m, 16H).

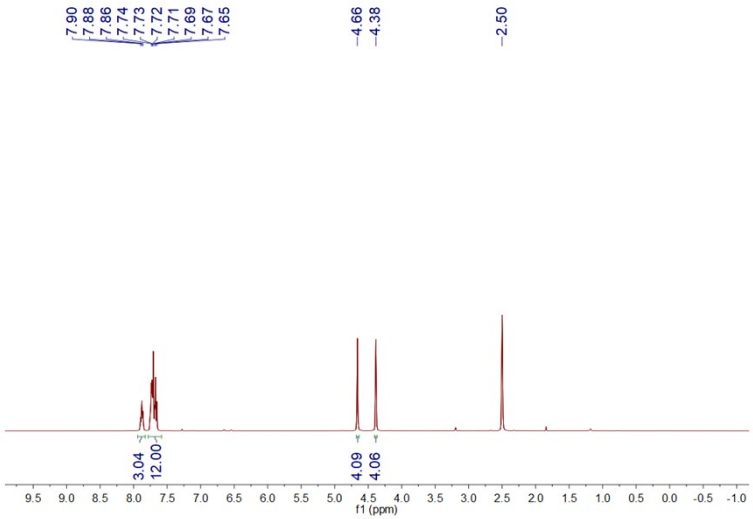

Figure S4. ^{1}H NMR spectra of the **1**: ^{1}H NMR (400 MHz, DMSO-d_6) δ 7.88 (t, J = 7.0 Hz, 3H, TPP^{+}), 7.74 – 7.65 (m, 12H, TPP^{+}), 4.66 (s, 4H, $FcDCA^{2-}$), 4.38 (s, 4H, $FcDCA^{2-}$).

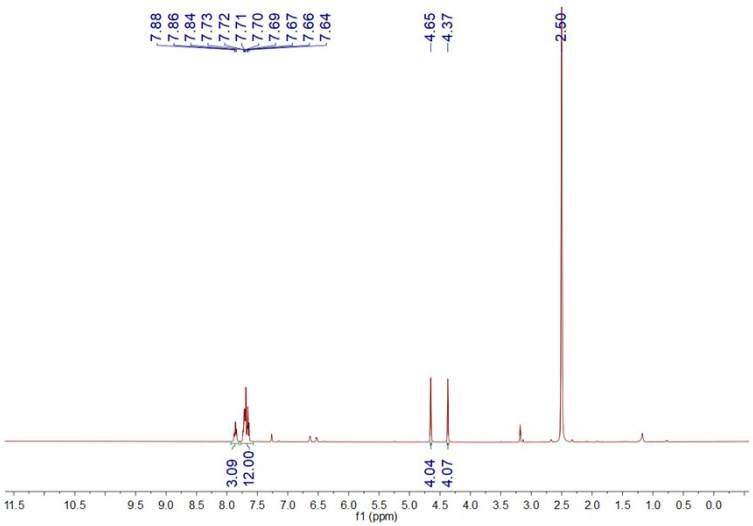

Figure S5. ^{1}H NMR spectra of the **2**: ^{1}H NMR (400 MHz, DMSO-d_6) δ 7.86 (t, J = 7.0 Hz, 3H, TPP^{+}), 7.73 – 7.64 (m, 12H, TPP^{+}), 4.65 (s, 4H, $FcDCA^{2-}$), 4.37 (s, 4H, $FcDCA^{2-}$).

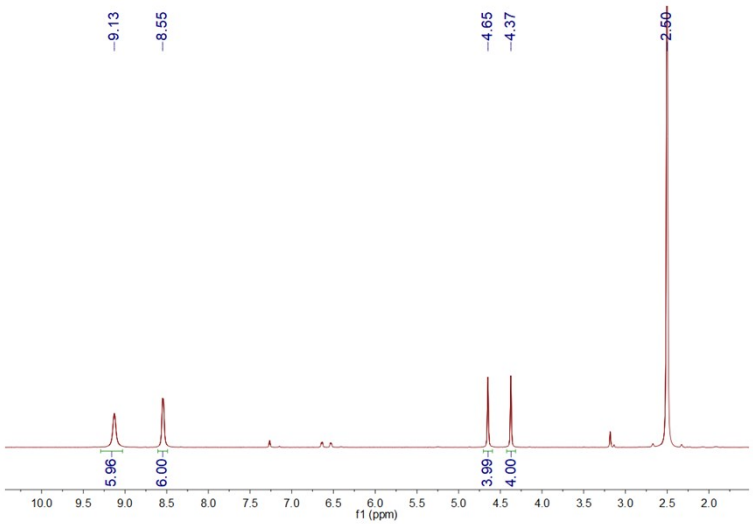

Figure S6. ^{1}H NMR spectra of the **3**: ^{1}H NMR (400 MHz, DMSO-d_6) δ 9.13 (s, 6H, bpy), 8.55 (s, 6H, bpy), 4.65 (s, 4H, $FcDCA^{2-}$), 4.37 (s, 4H, $FcDCA^{2-}$).

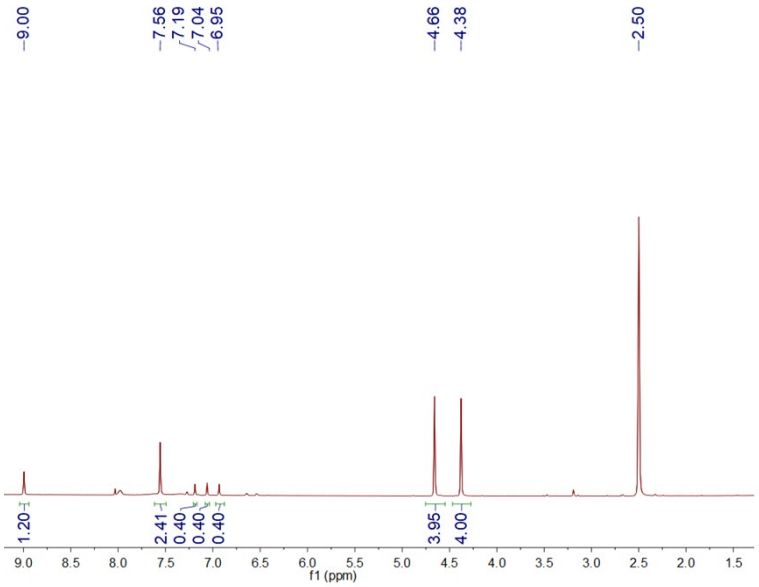

Figure S7. ^{1}H NMR spectra of the **4**.

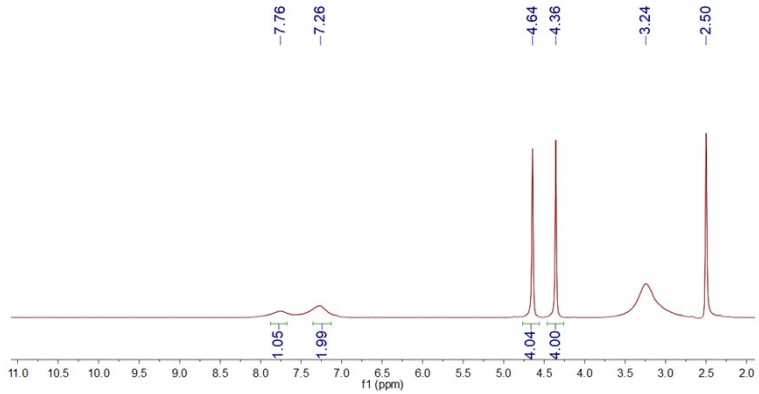

Figure S8. ^{1}H NMR spectra of the **7**: ^{1}H NMR (400 MHz, DMSO-d_6) δ 7.76 (s, 1H, Im^{-}), 7.26 (s, 2H, Im^{-}), 4.64 (s, 4H, $FcDCA^{2-}$), 4.36 (s, 4H, $FcDCA^{2-}$).

Fluorescence

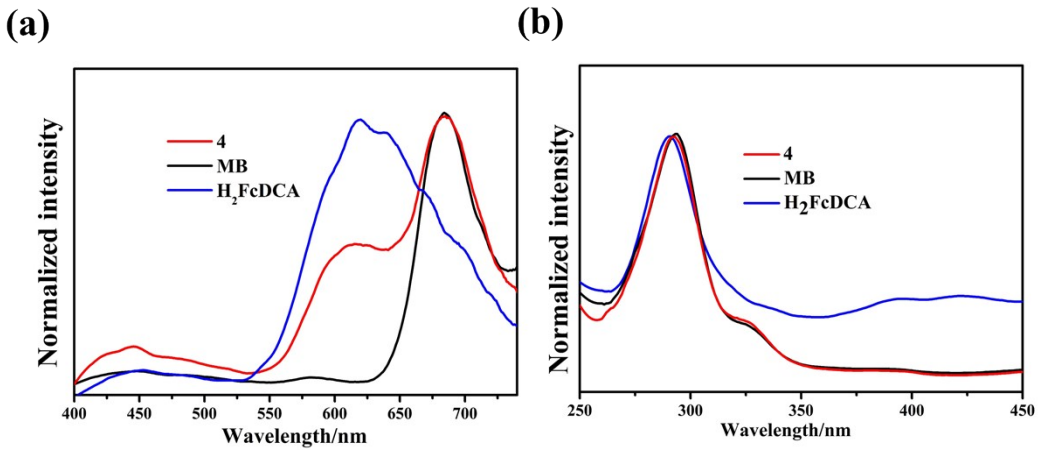

Figure S9. (a) Fluorescence emission (solid, λex = 295 nm) of **4**, H_2FcDCA, MB; (b) Fluorescence excitation (solid, λ_{em} = 690 nm) of **4**, H_2FcDCA, MB.

π- conjugated methylene blue has a strong absorption chromophore. We tested the fluorescence excitation and emission spectra of **4**, H_2FcDCA and MB at room temperature. The maximum excitation peaks of these three compounds are very close. Through 295 nm wavelength excitation, H_2FcDCA has weak fluorescence emission at about 600 nm, but MB has strong fluorescence emission at 690 nm, which is speculated to be generated by $\pi \rightarrow \pi^*$ transition. The emission peaks of **4** at 600 nm and 690 nm correspond to ligand and guest respectively, so their luminescence mechanism is the same.

Adsorption Characterization

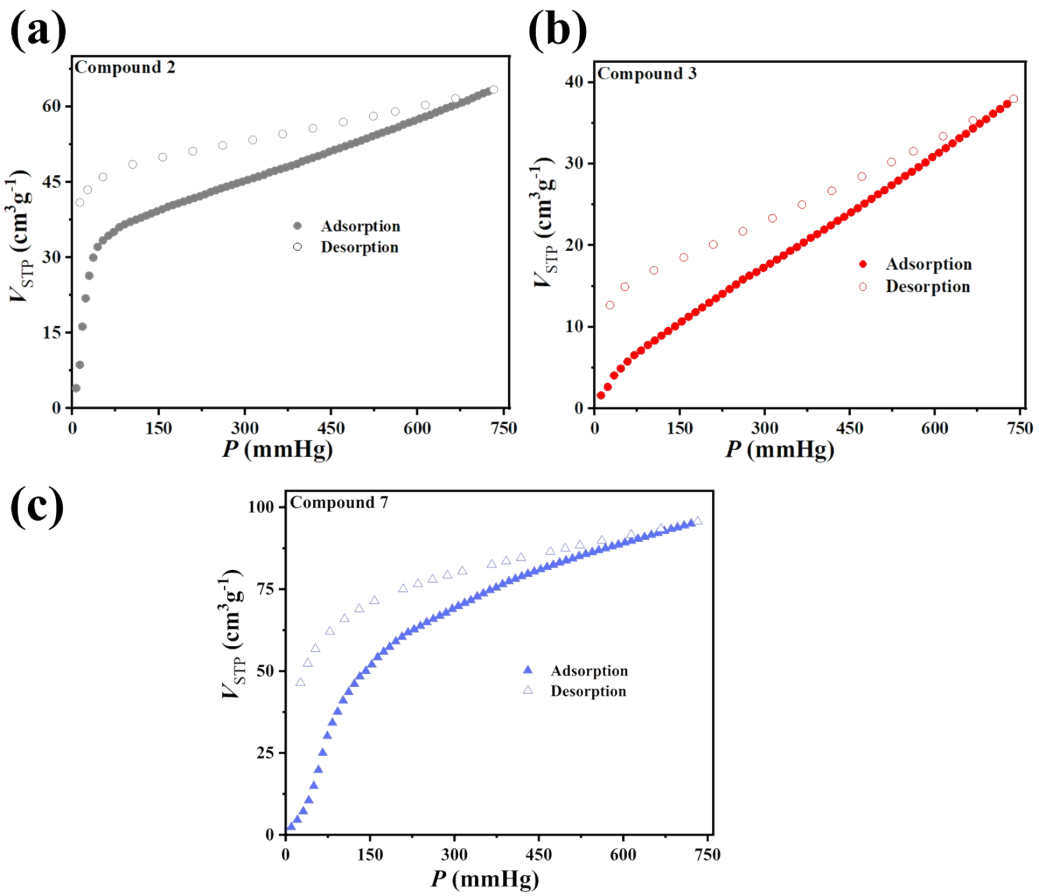

Figure S10. CO_2 adsorption at 195 K curves of **2** (a), **3** (b)**, 7** (d).

Activated compounds **2, 3** and **7**: **2** and **3** were degassed under a dynamic vacuum at 100 °C for 6 h to activate the sample, respectively. Freshly prepared sample of **7** were soaked in methanol and heated at 60 ℃. After 3 days, the guest formamide and polyethylene glycol was exchanged by methanol. Subsequently, **7** were degassed under a dynamic vacuum at 100 °C for 8 h to activate the sample. The permanent porosity of **2, 3** and **7** was confirmed by the CO_2-adsorption measurement at 195 K (Fig S10). The BET surface areas of **2, 3** and **7** were ~294 $m^2 \cdot g^{-1}$, ~306 $m^2 \cdot g^{-1}$ and ~510 $m^2 \cdot g^{-1}$ respectively, which is comparable to the recent results. [1, 2]

PXRD analyses

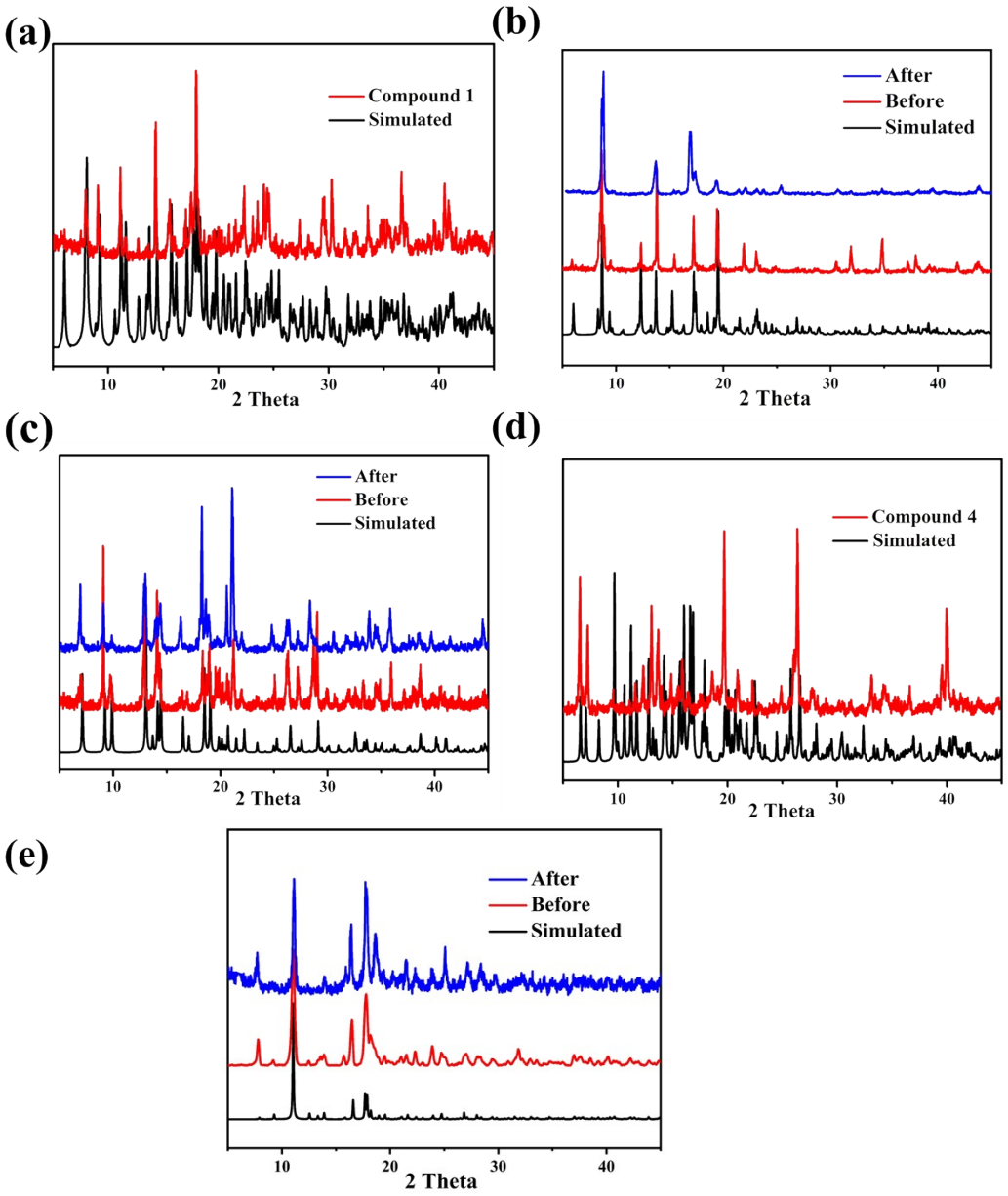

Figure S11. The PXRD patterns of compounds **1** (a) and **4** (d); PXRD of CO_2 adsorption of **2** (b) and **3** (c); PXRD of **7** before and after CO_2 adsorption tests.

TGA curves

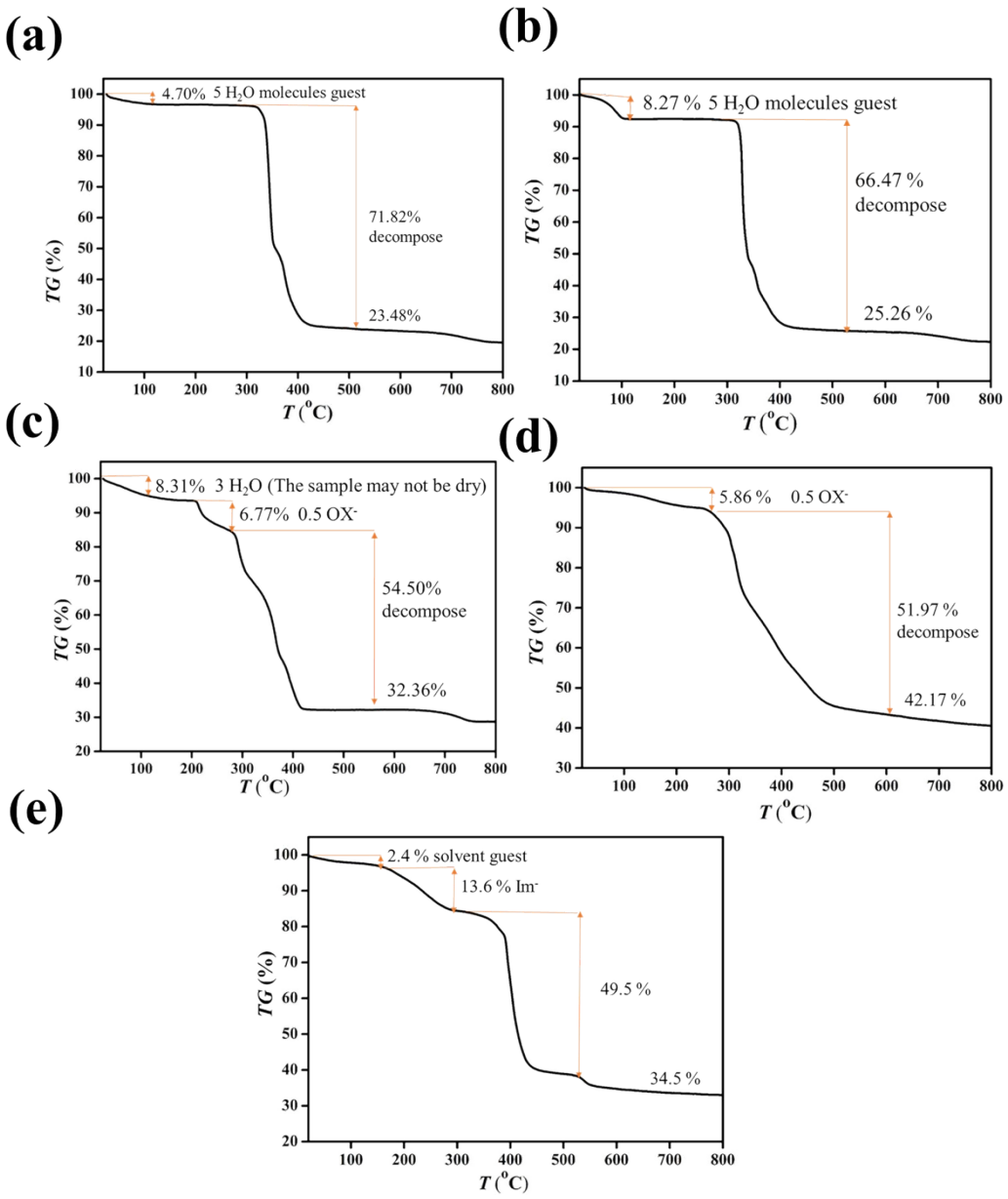

Figure S12. The TG plot of **1** (a), **2** (b), **3** (c),**4** (d) and **7** (e).

Calculation of the nonlinear optical parameters

The following values are calculated and simulated according to the reported literature. [3,4] I_0: the on-axis peak intensity at the focus (Z = 0), L_{eff}:the effective thickness of the sample, α is the linear absorption coefficient, and l is the sample thickness; n_0 is the refractive index of the medium (1.402); c: the speed of light; $Im\ \chi^{(3)}$: the imaginary

parts of the third-order susceptibility; *Re* $\chi^{(3)}$: the real parts of the third-order susceptibility; $\chi^{(3)}$:the absolute value of the third-order susceptibility.

$$T(Z,S=1)=\frac{1}{\pi^{\frac{1}{2}}(Z,0)}\int_{-\infty}^{\infty}\ln\left[1+q_0(Z,0)e^{-r^2}\right]dr \quad (1)$$

$$q_0(Z,0)=\beta I_0 L_{eff} \quad (2)$$

$$L_{eff}=\frac{1-e^{-\alpha l}}{\alpha} \quad (3)$$

$$\omega(Z)=\frac{\omega_0}{\left[1+\left(\frac{Z}{Z_0}\right)^2\right]^{-0.5}} \quad (4)$$

$$lm\chi^{(3)}(esu)=\left(\frac{c^2n_0^2\beta\left(m/W\right)}{240\pi^2\omega}\right) \quad (5)$$

$$Re\chi^{(3)}(esu)=\left(\frac{cn_0^2n_2\left(m^2/W\right)}{120\pi^2}\right) \quad (6)$$

$$|\chi^{(3)}|=\sqrt{|lm\chi^{(3)}|^2+|lm\chi^{(3)}|^2} \quad (7)$$

UV-Vis spectra

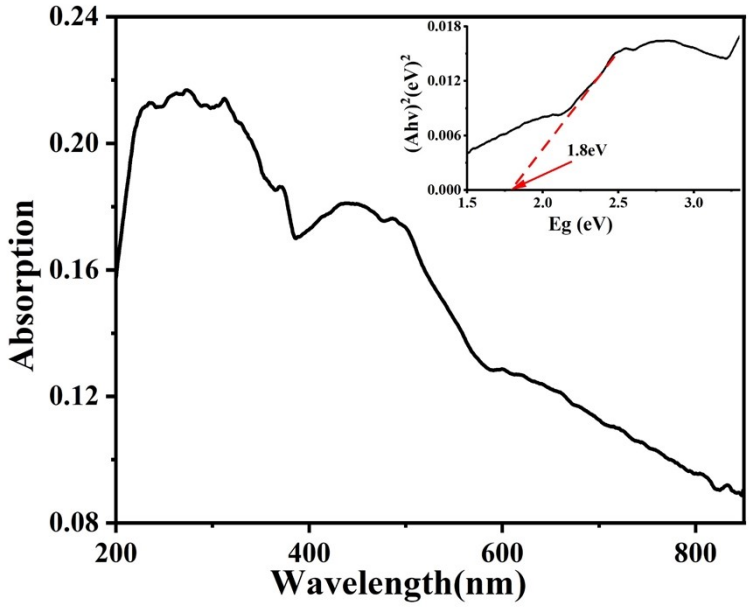

Figure S13. UV-Vis spectra of **1** and the band gap is 1.8 eV.

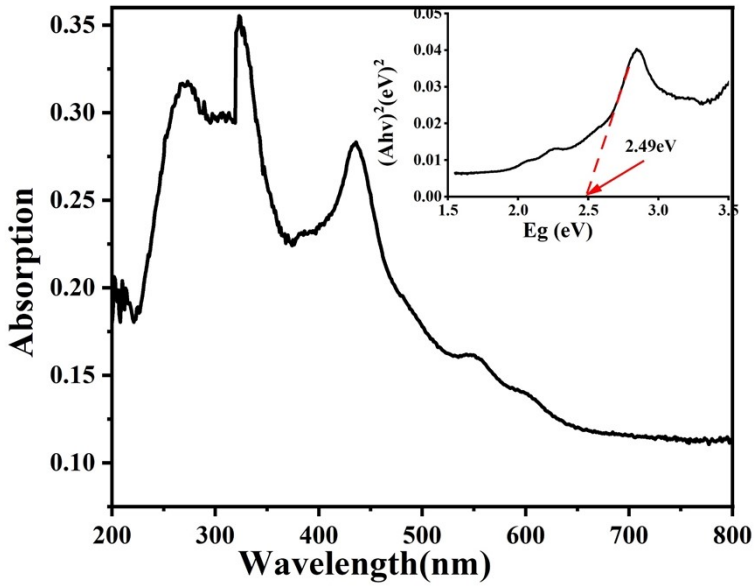

Figure S14. UV-Vis spectra of **2** and the band gap is 2.49 eV.

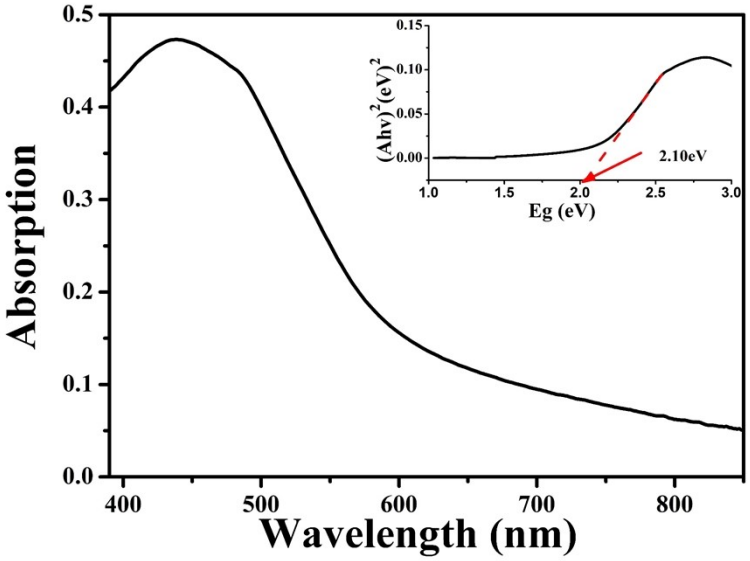

Figure S15. UV-Vis spectra of **3** and the band gap is 2.1 eV.

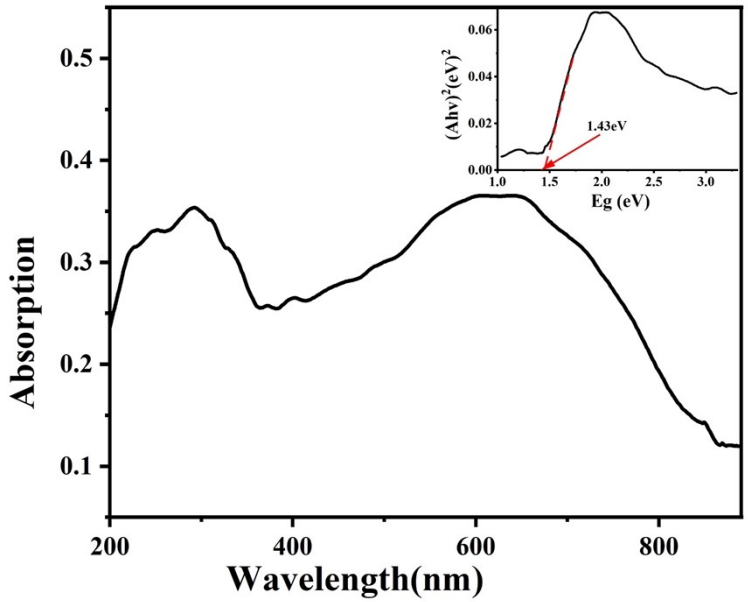

Figure S16. UV-Vis spectra of **4** and the band gap is 1.43 eV.

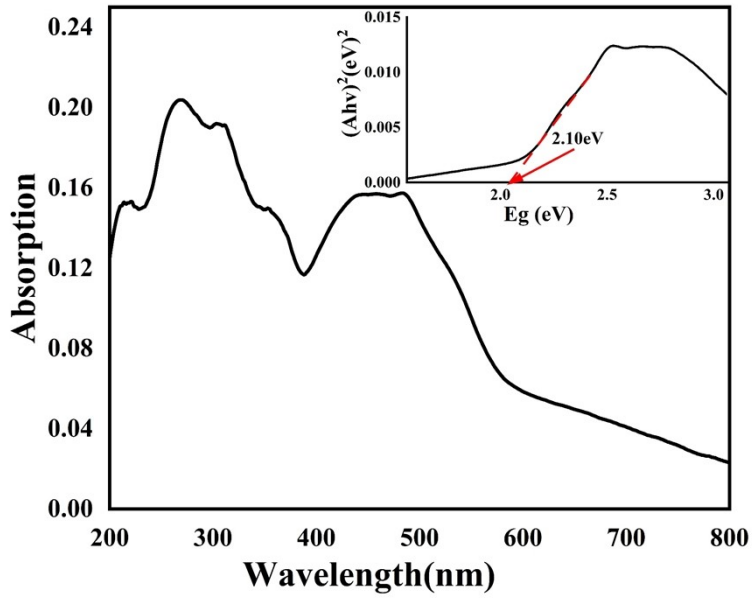

Figure S17. UV-Vis spectra of **7** and the band gap is 2.1 eV.

Cyclic voltammetric curves

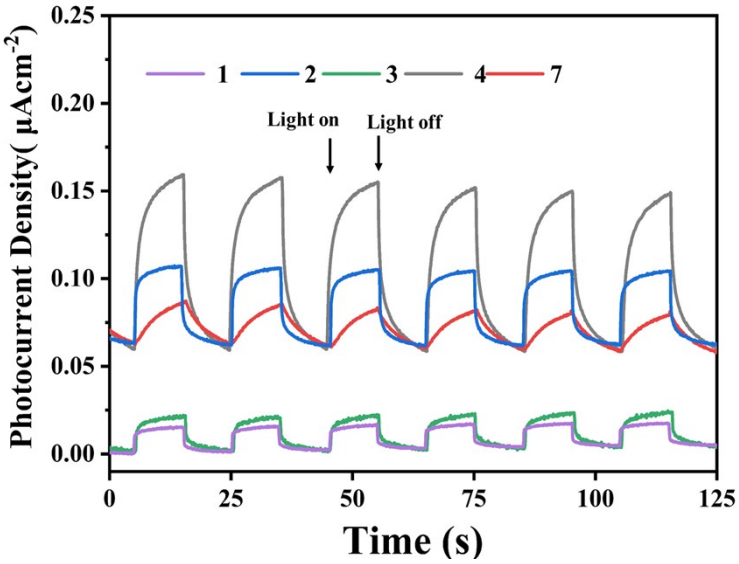

Figure S18. 0.2 V-bias photocurrent responses of electrodes derived for **1** to **4** and **7** in a 0.2 M Na_2SO_4 aqueous solution under repetitive chopped visible light irradiation.

Cyclic voltammetric curves

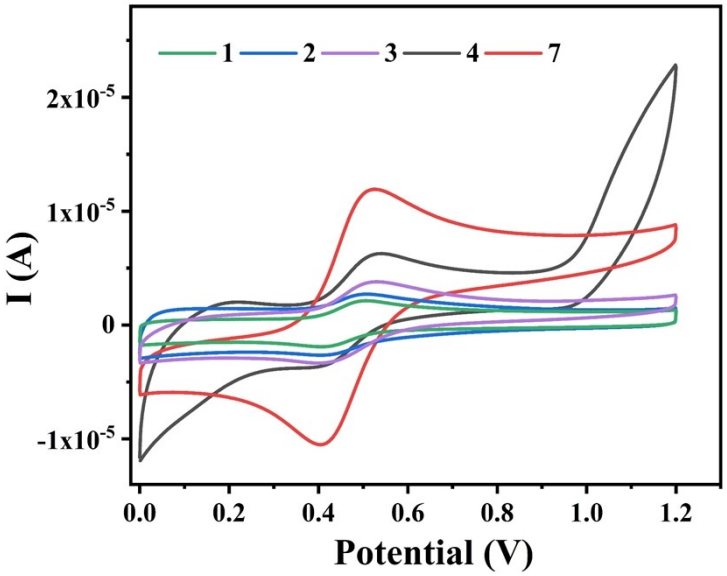

Figure S19.CV curves of **1** to **4** and **7** (20th cycle) on a cleaned FTO glass are shown.

References

1. R. Gao, S. M. Chen, F. Wang and J. Zhang, Single-Crystal Syntheses and Properties of Indium-Organic Frameworks Based on 1,1'-Ferrocenedicarboxylic Acid, *Inorg Chem*, 2021, **60**, 239-245.

2. J. Benecke, S. Mangelsen, T. A. Engesser, T. Weyrich, J. Junge, N. Stock and H. Reinsch, A porous and redox active ferrocenedicarboxylic acid based aluminium MOF with a MIL-53 architecture, *Dalton Trans*, 2019, **48**, 16737-16743.
3. D. -J. Li, Q. -H. Li, Z. -R. Wang, Z. -Z. Ma, Z. -G. Gu and J. Zhang, Interpenetrated Metal-Porphyrinic Framework for Enhanced Nonlinear Optical Limiting, *J Am Chem Soc*, 2021, **143**, 17162-17169.
4. Q. -F. Chen, X. Zhao, Q. Liu, J. D. Jia, X. -T. Qiu, Y. L. Song, D. J. Young, W. H. Zhang and J. P. Lang, Tungsten(VI)-Copper(I)-Sulfur Cluster-Supported Metal-Organic Frameworks Bridged by in Situ Click-Formed Tetrazolate Ligands, *Inorg Chem*, 2017, **56**, 5669-5679.